High thermoelectric performance in tellurium free p-type AgSbSe$_2$†

Satya N. Guin,[a] Arindom Chatterjee,[a] Devendra Singh Negi,[bc] Ranjan Datta[bc] and Kanishka Biswas*[a]

Enhanced electrical transport and ultra low thermal conductivity resulted in a high thermoelectric figure of merit, ZT, of ~1 and ~1.15 at ~680 K in 4 mol% Pb and 2 mol% Bi doped AgSbSe$_2$, which are 150 and 190% higher compared to that of the pristine sample, respectively. With this excellent thermoelectric performance, p-type AgSbSe$_2$, constituting earth abundant Se, offers promise to replace traditional metal tellurides containing expensive and scarce Te for mid temperature (350–700 K) thermoelectric applications.

Driven by the demand for clean and sustainable energy sources, thermoelectricity has become an important part of the research portfolio seeking to recognize new and efficient energy materials for power generation and cooling applications. Thermoelectric materials can directly and reversibly convert heat energy into electrical energy.[1] The efficiency of thermoelectric materials is quantified by a dimensionless figure of merit, ZT = $\sigma S^2 T/(\kappa_{el} + \kappa_{lat})$, where σ, S, T, κ_{el} and κ_{lat} are the electrical conductivity, Seebeck coefficient, temperature, electronic thermal conductivity and lattice thermal conductivity, respectively.[1] Among the high performance inorganic materials, PbTe is the most efficient for power generation applications at high temperature,[2–4] whereas Bi$_2$Te$_3$ based materials are well known for refrigeration near room temperature.[5] Beyond these traditional materials, cubic I–V–VI$_2$ (where I = Cu, Ag, Au or alkali metal; V = As, Sb, Bi; and VI = Se, Te) semiconductors are renowned for their intrinsically low κ_{lat} due to the strong

Broader context

Thermoelectric materials can directly and reversibly convert waste heat into electrical energy, and will play a significant role in future energy management. The main challenge in this field is to develop highly efficient, stable and inexpensive solid state materials. Leading high performance thermoelectric materials such as Bi$_2$Te$_3$, PbTe, and AgSbTe$_2$ are mainly based on tellurium, which is extremely scarce in the Earth crust. Hence, the Te price is likely to rise sharply if Te-based thermoelectric materials reach mass markets. Given that Te is 5000% more rare than Se and 500% more expensive, there is a compelling need to utilize tellurium-free, earth abundant thermoelectrics which can still achieve high ZT performance. AgSbSe$_2$, a homologue of AgSbTe$_2$, containing earth abundant elements, has attracted our attention for thermoelectric investigation due to its intrinsically low thermal conductivity. In this work, we show that the optimum concentrations of Pb and Bi act as effective p-type dopants and substantially increase the electrical conductivity, which results in a large increase in the power factor. With superior electronic transport and ultra low thermal conductivity, high ZT values of ~1 and ~1.15 at 680 K were achieved in AgSb$_{0.96}$Pb$_{0.04}$Se$_2$ and AgSb$_{0.98}$Bi$_{0.02}$Se$_2$, which offer the promise to replace traditional metal tellurides for mid temperature power generation.

anharmonicity of the bonding arrangements in these compounds.[6] Recent theoretical and experimental studies on a series of cubic bulk I–V–VI$_2$ compounds have shown that the lone pair on the group V element plays an important role in deforming the lattice vibration, which results in strong anharmonicity.[7] Fifty years ago, Rosi *et al.*[8] recognized AgSbTe$_2$, a typical member of the I–V–VI$_2$ family, to be an efficient p-type thermoelectric material with a ZT of 1.3 at 720 K. In recent years, AgSbTe$_2$ has been repeatedly studied to improve its performance further by the optimization of the carrier concentration through doping with various elements.[9] Interestingly, AgSbTe$_2$ alloys with GeTe (TAGS)[10] and PbTe (LAST-m)[11] showed extraordinary ZT values of ~1.5 at 750 K and ~1.8 at 800 K, respectively.

These leading high performance I–V–VI$_2$ materials are mainly based on tellurium which is extremely scarce in the Earth crust.[12] Hence the Te price is likely to rise sharply if

*a*New Chemistry Unit, Jawaharlal Nehru Centre for Advanced Scientific Research (JNCASR), Jakkur P.O., Bangalore 560064, India. E-mail: kanishka@jncasr.ac.in

*b*Chemistry and Physics of Materials Unit, Jawaharlal Nehru Centre for Advanced Scientific Research (JNCASR), Jakkur P.O., Bangalore 560064, India

*c*International Centre for Materials Science, Jawaharlal Nehru Centre for Advanced Scientific Research (JNCASR), Jakkur P.O., Bangalore 560064, India

† Electronic supplementary information (ESI) available: Experimental and measurement details; zoomed PXRD (Fig. S1); thermal diffusivity (Fig. S2); heat capacity (Fig. S3), Lorentz number for pristine AgSbSe$_2$ and Pb/Bi doped AgSbSe$_2$ samples (Fig. S4), ZT of samples with similar composition and annealed sample (Fig. S5) and heating–cooling cycle transport data (Fig. S6). See DOI: 10.1039/c3ee41935e

This journal is © The Royal Society of Chemistry 2013

Energy Environ. Sci., 2013, **6**, 2603–2608 | **2603**

Te-based thermoelectric materials reach mass markets. Therefore, it would be desirable to develop alternative materials which minimize the use of rare and toxic elements such as Te and involve cheaper and more abundant elements. Attractive alternatives are Pb free $AgBiSe_2$ and $AgSbSe_2$ because Se is less expensive, has a longer-term price stability, and is 50 times more abundant than Te. Recently, ZT values as high as ~1 at 773 K have been achieved in n-type Nb doped bulk $AgBiSe_2$ synthesized by a solid state reaction.[13] Solution grown nanocrystalline $AgBiSe_2$ also exhibits a high ZT of ~1.5 at 700 K with interesting p–n–p type conduction.[14] Recently, n-type $BiAgSeS_{1−x}Cl_x$ has also shown promising thermoelectric performance due to its low thermal conductivity.[15] It must be mentioned that Se based bulk $AgCrSe_2$ exhibits a ZT close to unity at 750 K due to the low thermal conductivity that arises from the disordering of the cation.[16]

$AgSbSe_2$, a homologue of $AgSbTe_2$, containing earth abundant elements, has attracted our attention for thermoelectric investigation due to its intrinsically low κ_{lat}.[7] At room temperature, $AgSbSe_2$ crystallizes in a cubic rock salt structure (space group, $Fm\bar{3}m$) with disordered Ag and Sb positions (Fig. 1(a))[17] and strong anharmonicity in the Sb–Se bond due to the presence of a stereochemically active $5s^2$ lone pair on Sb. In addition to low thermal conductivity, $AgSbSe_2$ is a narrow band gap

semiconductor with a favorable valence band structure composed of 12 half-pockets located at the X-point of the Brillouin zone.[9a,b,18] Thermoelectric performance of $AgSbSe_2$ can therefore be enhanced significantly by the convergence of many valleys through proper carrier engineering.[2]

Herein we report the synthesis and promising thermoelectric properties of high quality bulk crystalline ingots of p-type bulk $AgSbSe_2$ doped with 2–4 mol% Pb and Bi. We show that the optimum concentration of Pb acts as an effective p-type dopant and substantially increases the electrical conductivity, which results in a large increase in the power factor ($S^2\sigma$) of $AgSbSe_2$ over a broad temperature range. The large thermopower in this system was achieved due to the broad valence band maximum and multi-peak valence band structure of $AgSbSe_2$.[9a] We could achieve a maximum ZT of ~1 at 610 K in the case of the $AgSb_{0.96}Pb_{0.04}Se_2$ crystalline ingot due to its high power factor and ultra low thermal conductivity. Moreover, with optimum Bi doping, the ZT of p-type $AgSbSe_2$ can reach ~1.15 at 680 K, which is 190% higher than that of pristine $AgSbSe_2$.

Pristine $AgSbSe_2$ and nominally doped $AgSb_{1−x}Pb_xSe_2$ ($x = 0.02, 0.04$) and $AgSb_{1−x}Bi_xSe_2$ ($x = 0.02, 0.04$) bulk ingots (~9 g) were synthesized by adding appropriate ratios of high purity starting materials of Ag, Sb, Bi/Pb and Se to fused-silica tubes (~10 mm diameter). The tubes were sealed under high vacuum (~10^{-5} Torr) and slowly heated up to 673 K over 12 h, then to 1123 K over 4 h, soaked for 10 h, and subsequently cooled to room temperature (see Experimental section). In Fig. 1(b), we show a typical photograph of the "as-synthesized" high quality $AgSbSe_2$ ingot. Bar and coin shaped samples (Fig. 1(b)) obtained after cutting and polishing such ingots, were used for electrical and thermal transport measurements, respectively.

Powder X-ray diffraction patterns (XRD) (Fig. 1(c)) of the $AgSbSe_2$, $AgSb_{1−x}Pb_xSe_2$ ($x = 0.02, 0.04$) and $AgSb_{1−x}Bi_xSe_2$ ($x = 0.02, 0.04$) samples could be indexed on the cubic $AgSbSe_2$ structure (space group, $Fm\bar{3}m$) with no other impurity phase observed within the detection limits of powder XRD. The observed linear expansion in the lattice parameter follows Vegard's law for the $AgSb_{1−x}Pb_xSe_2$ ($x = 0.02, 0.04$) and $AgSb_{1−x}Bi_xSe_2$ ($x = 0.02, 0.04$) samples, with increasing Pb or Bi concentrations (Fig. 1(d) and (e)). The ionic radii of Bi and Pb are larger than that of Sb. As bigger Pb or Bi is introduced in the place of smaller Sb, the unit cell undergoes a systematic expansion, leading to an increase in the lattice parameter. This gradual expansion of lattice parameter indicates an isomorphic substitution of the smaller Sb position by bigger Pb or Bi.

The spectroscopically measured band gap of the bulk $AgSbSe_2$ is ~0.7 eV, which is typical of a narrow band gap semiconductor (Fig. 1(f)). The systematic decrease in the band gaps of $AgSb_{0.98}Pb_{0.02}Se_2$ and $AgSb_{0.98}Bi_{0.02}Se_2$, compared to pristine $AgSbSe_2$, supports the successful substitution of Pb or Bi in the Sb sublattice of $AgSbSe_2$. The absorption edge is not sharp and is suggestive of an indirect gap. This is consistent with the previous electronic band structure calculations for $AgSbSe_2$.[9a]

In order to understand the nanoscale architecture of the Pb/Bi doped $AgSbSe_2$, we have performed a transmission electron microscopy (TEM) investigation (Fig. 2). Fig. 2(a) shows the
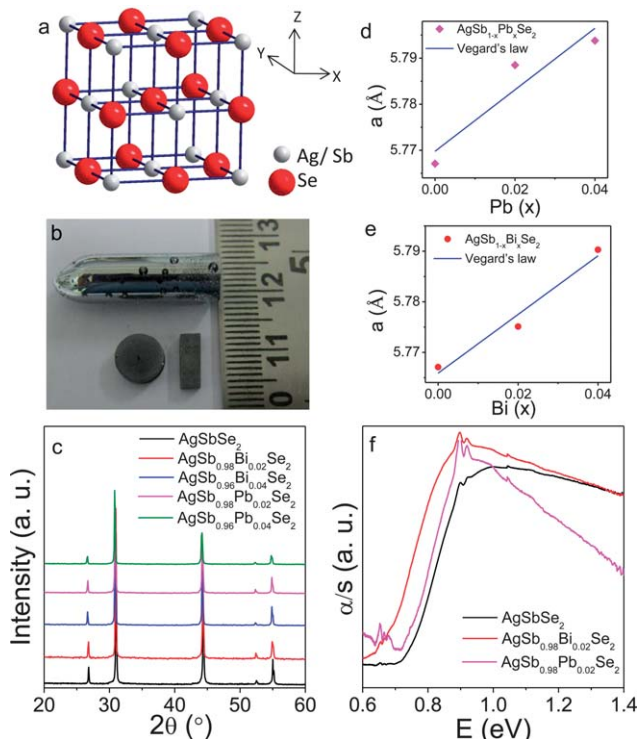
Fig. 1 (a) Crystal structure of cubic rocksalt $AgSbSe_2$ with disordered Ag/Sb positions. (b) Photograph of the as-synthesized ingot. Bar- and coin-shaped samples are used for electrical and thermal transport measurements, respectively. (c) Powder XRD patterns of pristine $AgSbSe_2$ and Pb or Bi doped $AgSbSe_2$ samples. (d) & (e) Lattice parameter (a) vs. Pb or Bi concentrations in $AgSb_{1−x}(Pb/Bi)_xSe_2$ ($x = 0.02, 0.04$) and the solid line indicates Vegard's law for a solid solution. (f) Electronic absorption spectra of $AgSbSe_2$ and 2 mol% Pb and Bi doped $AgSbSe_2$.

2604 | Energy Environ. Sci., 2013, **6**, 2603–2608

This journal is © The Royal Society of Chemistry 2013
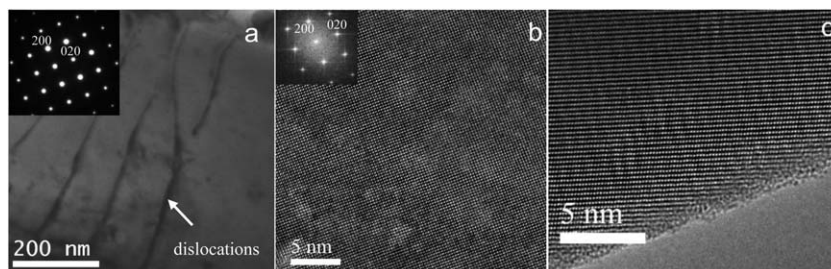
Fig. 2 (a) Low magnification TEM image of $AgSb_{0.98}Pb_{0.02}Se_2$; inset in (a) shows the electron diffraction pattern. High resolution TEM images of (b) $AgSb_{0.98}Pb_{0.02}Se_2$ and (c) $AgSb_{0.98}Bi_{0.02}Se_2$ samples. Inset in (b) shows the corresponding pattern obtained by a Fourier transformation.

low magnification TEM image of the $AgSb_{0.98}Pb_{0.02}Se_2$ sample. Although we have observed the presence of dislocations and grain boundaries, we have not observed the presence of nano-precipitates in the sample. This result suggests the solid solution nature of the samples, which also supports the XRD and band gap results. The electron diffraction pattern (inset, Fig. 2) confirms the single phase $AgSbSe_2$ with space group, $Fm\bar{3}m$. Fig. 2(b) and (c) show the high resolution TEM images of $AgSb_{0.98}Pb_{0.02}Se_2$ and $AgSb_{0.98}Bi_{0.02}Se_2$ samples.

The temperature dependent electrical properties of $AgSbSe_2$ and solid solution $AgSb_{1-x}Pb_xSe_2$ ($x = 0.02, 0.04$) samples over a 290–723 K range are presented in Fig. 3. The electrical conductivity (σ) and Seebeck coefficient (S) were measured simultaneously under a He atmosphere from room temperature to ∼723 K on a ULVAC-RIKO ZEM3 instrument (Experimental, ESI†). Fig. 3(a) shows the temperature-dependent σ of pristine $AgSbSe_2$ and $AgSb_{1-x}Pb_xSe_2$ ($x = 0.02, 0.04$) samples. The room temperature σ value measured for the pristine sample is ∼4.5 S cm^{-1}. A systematic rise of σ at room temperature is observed with increasing Pb doping concentrations from 0 to 4 mol%. Typically, the room temperature σ for the $AgSb_{0.96}Pb_{0.04}Se_2$ sample was ∼61 S cm^{-1}, which remains almost the same up to 600 K and then decreases to ∼16 S cm^{-1} at 705 K.

The Hall coefficient, R_H, at room temperature is positive for pristine and Pb doped samples, which indicates p-type conduction in this system. Assuming parabolic bands and a single band conduction process at 300 K, we estimated the carrier concentration, n, from the formula: $n = 1/eR_H$, where e is the electronic charge. The measured carrier concentrations are 5×10^{18} and 3×10^{19} carriers per cm^3 for the pristine $AgSbSe_2$ and $AgSb_{0.96}Pb_{0.04}Se_2$, respectively (Table 1). An increase in the hole concentration in Pb doped samples indicates that the Pb^{2+} is doped on the Sb^{3+} cation sublattice and, from simple valence counting, contributes one p-type carrier. The room temperature hole mobility, defined as $\mu = \sigma/ne$, for pristine $AgSbSe_2$ and $AgSb_{0.96}Pb_{0.04}Se_2$ samples is ∼7 and ∼13 cm^2 V^{-1} s^{-1}, respectively (Table 1). A low hole mobility indicates the presence of heavy holes, resulting from the flat valence band maximum of $AgSbSe_2$.[9a]

Fig. 3(b) shows the temperature dependent Seebeck coefficient of $AgSbSe_2$ and Pb doped $AgSbSe_2$. A positive value of S confirms the p-type conduction in the system. The room temperature S value measured for pristine $AgSbSe_2$ was ∼310 µV K^{-1}, which linearly increases to ∼461 µV K^{-1} at 705 K. The flat

valence band maximum and multipeak valence band structure result in a large positive thermopower in this compound.[9a] In the case of $AgSb_{0.98}Pb_{0.02}Se_2$ and $AgSb_{0.96}Pb_{0.04}Se_2$ samples, the room temperature S values are ∼220 and ∼215 µV K^{-1}, respectively, which increase to ∼405 and ∼400 µV K^{-1}, respectively at 705 K. The high S values in this compound may be due to the high density of state effective mass (m^*). Assuming a single parabolic band model with acoustic phonon scattering
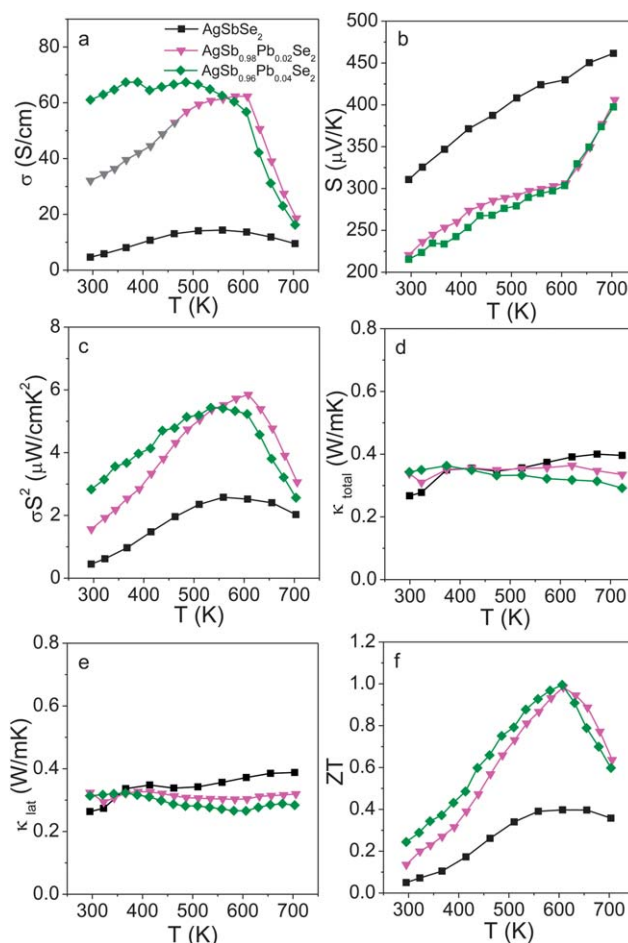
Fig. 3 Temperature-dependent (a) electrical conductivity (σ), (b) Seebeck coefficient (S), (c) power factor (σS^2), (d) total thermal conductivity (κ_{total}), (e) lattice thermal conductivity (κ_{lat}), and (f) thermoelectric figure of merit (ZT) of $AgSb_{1-x}Pb_xSe_2$ ($x = 0.02, 0.04$) and pristine $AgSbSe_2$.

Table 1 Carrier concentration (n), electrical conductivity (σ) and carrier mobility (μ) of pristine AgSbSe$_2$, selected Pb and Bi doped AgSbSe$_2$ samples at room temperature

Sample	n (cm^{-3})	σ (S cm^{-1})	μ (cm^2 V^{-1} s^{-1})
AgSbSe$_2$	5×10^{18}	5	7
AgSb$_{0.98}$Bi$_{0.02}$Se$_2$	1.5×10^{19}	51	22
AgSb$_{0.96}$Pb$_{0.04}$Se$_2$	3×10^{19}	61	13

($r = -1/2$), we have estimated the m^* according to the following eqn (1–3) using the measured S and Hall carrier concentration (n):[9b,d,15]

$$m^* = \frac{h^2}{2k_B T}\left[\frac{n}{4\pi F_{1/2}(\eta)}\right]^{2/3} \tag{1}$$

$$S = \pm\frac{k_B}{e}\left(\frac{(r+3/2)F_{r+3/2}(\eta)}{(r+3/2)F_{r+1/2}(\eta)} - \eta\right) \tag{2}$$

$$F_n(\eta) = \int_0^\infty \frac{x^n}{1+e^{x-\eta}}\,dx \tag{3}$$

where, η is the reduced Fermi energy, $F_n(\eta)$ is the nth order Fermi integral, k_B is the Boltzmann constant, e is the electron charge, h is the Planck constant and r is the scattering factor. The reduced Fermi energy was extracted based on fitting the respective Seebeck data.[15,19] The calculation gives an m^* of $1.2m_0$ and $1.8m_0$ for pristine AgSbSe$_2$ and AgSb$_{0.98}$Pb$_{0.02}$Se$_2$, respectively. Similar m^* values of $1.7 \pm 0.2m_0$ were obtained by Jovovic and Heremans in the case of AgSbTe$_2$ with a similar p-type carrier density, 3×10^{19} carriers per cm^3.[9b] Wojcie-chowski et al. also obtained a high m^* of $2.7m_0$ for AgSbTe$_2$ with the carrier density of 5×10^{19} carriers per cm^3.[20] m^* values of 0.21–$0.85m_0$ were observed in solid solution AgSbTe$_{2-x}$Se$_x$ which has comparatively lower carrier concentrations. Optimum Pb doping in AgSbSe$_2$ increases the number of p-type carriers markedly (Table 1). We speculate that at high temperatures, high density carriers resulted from heavy doping may be redistributed in the multiple degenerate valence bands, thus giving rise to the effective convergence of bands.[2] An increase in the population of carriers in the multiple flat valence bands at high temperature produces higher m^*, which in turn results in an increase in S above 600 K (Fig. 3(b)), as S is directly related to m^* by eqn (4)[1a,b]

$$S = \frac{8\pi^2 k_B^2}{3eh^2}m^* T\left(\frac{\pi}{3n}\right)^{3/2} \tag{4}$$

We have already observed that these compounds have a low hole mobility, which is due to the presence of heavy holes (Table 1). The probable increase in m^* at high temperatures further decreases the hole mobility, thus resulting in a decrease in σ (Fig. 3(a)) above 600 K for Pb-doped samples.

Power factor (σS^2) values for AgSb$_{1-x}$Pb$_x$Se$_2$ ($x = 0.02, 0.04$) samples are markedly higher than pristine AgSbSe$_2$ (Fig. 3(c)). Typically, the room temperature σS^2 value is $\sim$1.6 µW cm^{-1} K^{-2}

for the 2 mol% Pb doped sample. This value rises to a maximum of $\sim$5.9 µW cm^{-1} K^{-2} at about 610 K and falls to $\sim$3.1 µW cm^{-1} K^{-2} at $\sim$710 K.

The total thermal conductivity, κ_{total}, of the samples was estimated to be in the temperature range of 300–725 K using the formula, $\kappa_{total} = DC_p\rho$, where D is the thermal diffusivity, C_p is the specific heat and ρ is the density of the sample. D is measured by a laser flash diffusivity technique by using a NETZSCH LFA 457 instrument over a 300–725 K range. At room temperature, a typical κ_{total} value of $\sim$0.35 W m^{-1} K^{-1} was observed for the AgSb$_{0.96}$Pb$_{0.04}$Se$_2$ sample, which remains almost the same throughout the 300–725 K range (Fig. 3(d)). The lattice thermal conductivity, κ_{lat}, was obtained after subtracting the electronic part, κ_e from the κ_{total} and is plotted in Fig. 3(e). The electronic thermal conductivities, $\kappa_e = L\sigma T$, were extracted based on fitting of the respective Seebeck values which estimate the reduced chemical potential from which the Lorentz number, L, can be obtained, as explained in detail previously.[19] This assumes a parabolic band model and energy independent scattering time. Calculated Lorentz numbers for different AgSbSe$_2$ samples are given in Fig. S4 (ESI†). Typically, the AgSb$_{0.96}$Pb$_{0.04}$Se$_2$ sample exhibits a κ_{lat} value of $\sim$0.3 W m^{-1} K^{-1} at room temperature, which remains almost the same in the 300–725 K range. This extremely low κ_{lat} value observed in this system is due to two possible reasons: (a) the high degree of anharmonicity of the Sb–Se bonds that gives rise to strong phonon–phonon interactions and (b) effective phonon scattering by the highly disordered Ag/Sb lattice.

Fig. 3(f) presents the ZT values of pristine AgSbSe$_2$ and samples doped with 2–4 mol% Pb. The maximum ZT achieved is $\sim$1 at 610 K for both 2% and 4% Pb doped samples, which is 150% higher compared to pristine AgSbSe$_2$.

We have also measured the electronic and thermal transport properties of AgSb$_{1-x}$Bi$_x$Se$_2$ ($x = 0.02, 0.04$) samples in the 300–725 K range (Fig. 4). Typically, the room temperature σ for the AgSb$_{0.98}$Bi$_{0.02}$Se$_2$ sample was $\sim$51 S cm^{-1} which remains almost the same up to 655 K, then decreases to $\sim$35 S cm^{-1} at 705 K (Fig. 4(a)). The Hall coefficient, R_H, is positive for Bi doped samples, indicating they are p-type carriers. The carrier concentration estimated from R_H is $\sim$1.5 $\times$ 10^{19} carriers per cm^3 for AgSb$_{0.98}$Bi$_{0.02}$Se$_2$ (Table 1). The sign of S is also positive, which confirms the hole conduction (Fig. 4(b)). Typically, the room temperature S for the AgSb$_{0.98}$Bi$_{0.02}$Se$_2$ sample was $\sim$254 µV K^{-1}, which reaches $\sim$373 µV K^{-1} at 705 K. The density of state effective mass (m^*) of the AgSb$_{0.98}$Bi$_{0.02}$Se$_2$ sample was calculated to be 1.6m_0 using eqn (1–3). The highest room temperature σS^2 value of $\sim$3.4 µW cm^{-1} K^{-2} was achieved for the 4% Bi doped sample, which rises to $\sim$6.7 µW cm^{-1} K^{-2} at 660 K and then decreases to $\sim$4.9 µW cm^{-1} K^{-2} at 705 K (Fig. 4(c)). Power factors of AgSb$_{1-x}$Bi$_x$Se$_2$ samples are generally superior compared to AgSb$_{1-x}$Pb$_x$Se$_2$ samples. We have also observed ultra low κ_{total} values in the case of AgSb$_{1-x}$Bi$_x$Se$_2$ samples, similar to AgSb$_{1-x}$Pb$_x$Se$_2$. A typical room temperature value of κ_{total} $\sim$0.32 W m^{-1} K^{-1} was observed for the AgSb$_{0.98}$Bi$_{0.02}$Se$_2$ sample, which remains almost the same throughout the 300–725 K range (Fig. 4(d)).

2606 | *Energy Environ. Sci.*, 2013, **6**, 2603–2608

This journal is © The Royal Society of Chemistry 2013
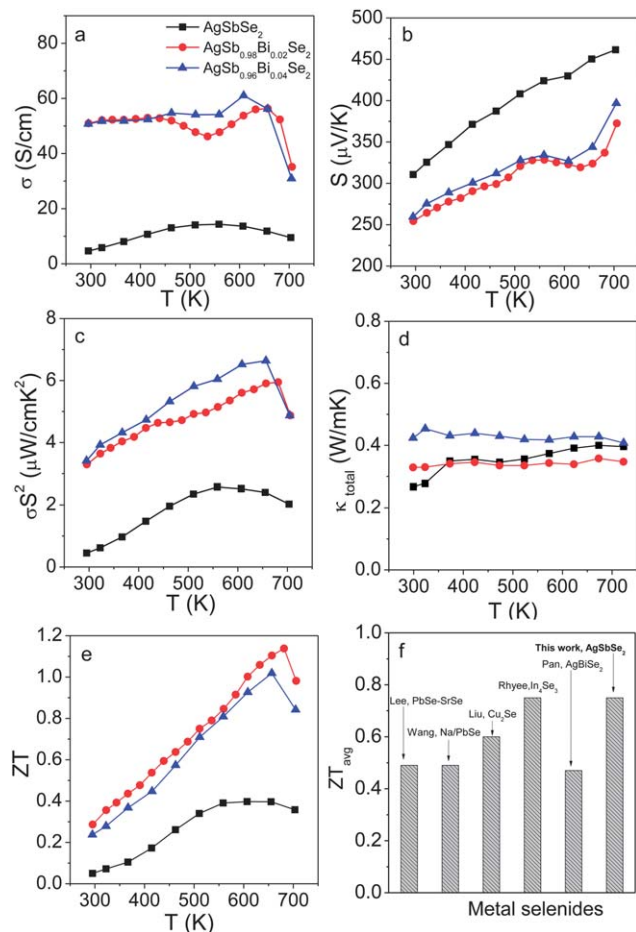
Fig. 4 Temperature-dependent (a) electrical conductivity (σ), (b) Seebeck coefficient (S), (c) power factor (σS^2), (d) total thermal conductivity (κ_{total}), and (e) thermoelectric figure of merit (ZT) of $AgSb_{1-x}Bi_xSe_2$ (x = 0.02, 0.04) and pristine $AgSbSe_2$. (f) Average ZT of the present $AgSb_{0.98}Bi_{0.02}Se_2$ and leading metal selenides reported in recent literature, considering a hot side temperature of 690 K and cold side temperature of 350 K.

From the electrical and thermal transport measurements, we have estimated the ZT of $AgSb_{1-x}Bi_xSe_2$ (x = 0.02, 0.04) samples in 300–710 K range (Fig. 4(e)). The maximum ZT achieved is ~1.15 at 685 K for the 2 mol% Bi doped sample, which is 190% higher compared to the pristine $AgSbSe_2$ sample. With this advance in the maximum ZT value of this Te-free material, we can expect an average ZT value of ~0.75 (considering a hot side temperature of 690 K and cold temperature of 350 K), which is comparable or higher than leading metal selenide based thermoelectric systems reported recently in the literature (Fig. 4(f)).[13,21]

In summary, high quality crystalline ingots of p-type $AgSbSe_2$, solid solution $AgSb_{1-x}Pb_xSe_2$ (x = 0.02, 0.04) and $AgSb_{1-x}Bi_xSe_2$ (x = 0.02, 0.04) were grown by simple melting of the elemental metal and chalcogen followed by quenching to room temperature. Hole concentrations in $AgSbSe_2$ could be optimized by doping of a small amount of Pb and Bi to achieve superior electrical conductivity compared to the pristine sample. The broad valence band maximum and multi-peak valence band structure resulted in a large thermopower in

$AgSbSe_2$. A high degree of anharmonicity in the Sb–Se bond and effective phonon scattering by the highly disordered Ag/Sb lattice gives rise to an ultra low κ_{lat}. Peak ZT values of ~1 and ~1.15 were achieved in $AgSb_{0.96}Pb_{0.04}Se_2$ and $AgSb_{0.98}Bi_{0.02}Se_2$ samples, which are 150% and 190% higher than that of pristine $AgSbSe_2$, respectively. With this excellent thermoelectric performance, p-type $AgSbSe_2$, consisting of earth abundant Se, offers a promise to replace traditional metal tellurides constituting expensive and scarce Te. The best ZT_{avg} found for our system is also in line with other leading metal selenide based thermoelectric materials in the mid temperature range (350–700 K). The performance of this system can be improved further by introducing nanoscale precipitates and mesoscale grain boundaries which can enhance phonon scattering.

Methods

Synthesis

Ingots (~9 g) of $AgSb_{1-x}Bi_xSe_2$ (x = 0.02, 0.04), $AgSb_{1-x}Pb_xSe_2$ (x = 0.02, 0.04) and pristine $AgSbSe_2$ were synthesized by mixing appropriate ratios of high-purity starting materials of Ag, Sb, Bi or Pb and Se in a quartz tube. The tubes were sealed under high vacuum (10^{-5} Torr) and slowly heated up to 673 K over 12 h, then heated up to 1123 K over 4 h, soaked for 10 h, and subsequently air cooled to room temperature.

Characterizations

Powder XRD for all the samples were recorded using Cu K$_\alpha$ (λ = 1.5406 Å) radiation on a Bruker D8 diffractometer. To probe the optical energy gap of these compounds, optical diffuse reflectance measurements were performed on finely ground powders using a Perkin Elmer Lambda 900, UV-vis/NIR spectrometer at room temperature. TEM imaging was performed using an aberration corrected FEI TITAN3TM 80–300 kV transmission electron microscope operating at 300 kV.

Thermoelectric measurements

σ and S were measured simultaneously on a sample of the dimensions 2 mm × 3 mm × 8 mm, under a helium atmosphere from 290 K to 723 K by a ULVAC-RIKO ZEM-3 instrument. The longer direction of the sample coincides with the direction in which the thermal conductivity was measured. Carrier concentrations were determined using Hall coefficient measurements at room temperature with an ECOPIA HMS 3000 system. Thermal diffusivity, D, was directly measured and heat capacity, C_p, was indirectly derived using a standard sample (pyroceram) in the range 298–723 K by using a laser flash diffusivity method in a Netzsch LFA-457. Coins with a diameter of 8 mm and a thickness of 2 mm were used in these measurements. κ_{total} was estimated using the formula, $\kappa_{total} = DC_p\rho$, where ρ is the density of the sample, measured from the sample dimensions and mass. ZT obtained on multiple samples with the same nominal composition displays excellent consistency and homogeneity (Fig. S5, ESI†). Heating and cooling cycles give repeatable transport properties for a given sample, which confirms the high temperature stability of the samples (Fig. S6, ESI†).

Acknowledgements

Notes and references

1 (a) J. Sootsman, D. Y. Chung and M. G. Kanatzidis, *Angew. Chem., Int. Ed.*, 2009, **48**, 8616; (b) G. J. Snyder and E. S. Toberer, *Nat. Mater.*, 2008, **7**, 105; (c) G. Chen, M. S. Dresselhaus, G. Dresselhaus, J. P. Fleurial and T. Caillat, *Int. Mater. Rev.*, 2003, **48**, 45; (d) J.-F. Li, W.-S. Liu, L.-D. Zhao and M. Zhou, *NPG Asia Mater.*, 2010, **2**, 152; (e) T. M. Tritt, *Annu. Rev. Mater. Res.*, 2011, **41**, 433; (f) K. Nielsch, J. Bachmann, J. Kimling and H. Böttner, *Adv. Energy Mater.*, 2011, **1**, 713.

2 (a) Y. Pei, X. Shi, A. La Londe, H. Wang, L. Chen and G. J. Snyder, *Nature*, 2011, **473**, 66; (b) Y. Pei, H. Wang and G. J. Snyder, *Adv. Mater.*, 2012, **24**, 6125.

3 (a) K. Biswas, J. He, I. D. Blum, C. I. Wu, T. P. Hogan, D. N. Seidman, V. P. Dravid and M. G. Kanatzidis, *Nature*, 2012, **489**, 414; (b) K. Biswas, J. He, Q. Zhang, G. Wang, C. Uher, V. P. Dravid and M. G. Kanatzidis, *Nat. Chem.*, 2011, **3**, 160; (c) K. Biswas, J. Q. He, G. Wang, S. H. Lo, C. Uher, V. P. Dravid and M. G. Kanatzidis, *Energy Environ. Sci.*, 2011, **4**, 4675.

4 J. P. Heremans, V. Jovovic, E. S. Toberer, A. Saramat, K. Kurosaki, A. Charoenphakdee, S. Yamanaka and G. J. Snyder, *Science*, 2008, **321**, 554.

5 (a) B. Poudel, Q. Hao, Y. Ma, Y. Lan, A. Minnich, B. Yu, X. Yan, D. Wang, A. Muto, D. Vashaee, X. Chen, J. Liu, M. S. Dresselhaus, G. Chen and Z. Ren, *Science*, 2008, **320**, 634; (b) R. J. Mehta, Y. Zhang, C. Karthik, B. Singh, R. W. Siegel, T. B. Tasciuc and G. Ramanath, *Nat. Mater.*, 2012, **11**, 233.

6 D. T. Morelli, V. Jovovic and J. P. Heremans, *Phys. Rev. Lett.*, 2008, **101**, 035901.

7 M. D. Nielsen, V. Ozolins and J. P. Heremans, *Energy Environ. Sci.*, 2013, **6**, 570.

8 F. D. Rosi, E. F. Hockings and N. E. Lindenblad, *RCA Rev.*, 1961, **22**, 82.

9 (a) K. Hoang, S. D. Mahanti, J. R. Salvador and M. G. Kanatzidis, *Phys. Rev. Lett.*, 2007, **99**, 156403; (b) V. Jovovic and J. P. Heremans, *Phys. Rev. B: Condens. Matter Mater. Phys.*, 2008, **77**, 245204; (c) V. Jovovic and J. P. Heremans, *J. Electron. Mater.*, 2009, **38**, 1504; (d) K. T. Wojciechowski and M. Schmidt, *Phys. Rev. B: Condens. Matter Mater. Phys.*, 2009, **79**, 184202; (e) B. L. Du, H. Li, J. J. Xu, X. F. Tang and C. Uher, *Chem. Mater.*, 2010, **22**, 5521.

10 S. H. Yang, T. J. Zhu, T. Sun, J. He, S. N. Zhang and X. B. Zhao, *Nanotechnology*, 2008, **19**, 245707.

11 K. F. Hsu, S. Loo, F. Guo, W. Chen, J. S. Dyck, C. Uher, T. Hogan, E. K. Polychroniadis and M. G. Kanatzidis, *Science*, 2004, **303**, 818.

12 Z. C. Hu and S. Gao, *Chem. Geol.*, 2008, **253**, 205.

13 L. Pan, D. Berardan and N. Dragoe, *J. Am. Chem. Soc.*, 2013, **135**, 4914.

14 (a) C. Xiao, X. Qin, J. Zhang, R. An, J. Xu, K. Li, B. Cao, J. Yang, B. Ye and Y. Xie, *J. Am. Chem. Soc.*, 2012, **134**, 18460; (b) C. Xiao, J. Xu, B. Cao, K. Li, M. Kong and Y. Xie, *J. Am. Chem. Soc.*, 2012, **134**, 7971.

15 Y. L. Pei, H. Wu, J. Sui, J. Li, D. Berardan, C. Barreteau, L. Pan, N. Dragoe, W.-S. Liu, J. He and L. D. Zhao, *Energy Environ. Sci.*, 2013, **6**, 1750.

16 (a) F. Gascoin and A. Maigan, *Chem. Mater.*, 2011, **23**, 2510; (b) A. Maigan, E. Guilmeau, F. Gascoin, Y. Breard and V. Hardy, *Sci. Technol. Adv. Mater.*, 2012, **13**, 053003.

17 S. Geller and J. H. Wernick, *Acta Crystallogr.*, 1959, **12**, 46.

18 K. Wojciechowski, M. Schmidt, J. Tobola, M. Koza, A. Olech and R. Zybaia, *J. Electron. Mater.*, 2010, **39**, 2053.

19 (a) L.-D. Zhao, S.-H. Lo, J. He, H. Li, K. Biswas, J. Androulakis, C.-I. Wu, T. P. Hogan, D. Y. Chung, V. P. Dravid, I. Todorov, D. Y. Chung and M. G. Kanatzidis, *J. Am. Chem. Soc.*, 2011, **133**, 20476; (b) J. Androulakis, I. Todorov, J. He, D. Y. Chung, V. P. Dravid and M. G. Kanatzidis, *J. Am. Chem. Soc.*, 2011, **133**, 10920.

20 K. Wojciechowski, J. Tobola, M. Schmidt and R. Zybaia, *J. Phys. Chem. Solids*, 2008, **69**, 2748.

21 (a) Y. Lee, S.-H. Lo, J. Androulakis, C.-I. Wu, L.-D. Zhao, D.-Y. Chung, T. P. Hogan, V. P. Dravid and M. G. Kanatzidis, *J. Am. Chem. Soc.*, 2013, **135**, 5152; (b) H. Wang, Y. Pei, A. D. LaLonde and G. J. Snyder, *Adv. Mater.*, 2011, **23**, 1366; (c) H. Liu, X. Shi, F. Xu, L. Zhang, W. Zhang, L. Chen, Q. Li, C. Uher, T. Day and G. J. Snyder, *Nat. Mater.*, 2012, **11**, 422; (d) J. S. Ryee, K. H. Lee, S. M. Lee, E. Cho, S. I. Kim, E. Lee, Y. S. Kwon, J. H. Shim and J. Kotliar, *Nature*, 2009, **459**, 965.